ADVANCES IN ATMOSPHERIC SCIENCES, 2024

• Original Paper •

Comparison and Verification of Coherent Doppler Wind Lidar and Radiosonde Data in the Beijing Urban Area

Zexu LUO[1], Xiaoquan SONG[*1,2], Jiaping YIN[3], Zhichao BU[4], Yubao CHEN[4], Yongtao YU[5], and Zhenlu ZHANG[6]

[1]*College of Marine Technology, Faculty of Information Science and Engineering, Ocean University of China, Qingdao* 266100, *China*

[2]*Laboratory for Regional Oceanography and Numerical Modeling, Laoshan Laboratory, Qingdao* 266237, *China*

[3]*Qingdao Leice Transient Technology Co. LTD, Qingdao* 266100, *China*

[4]*CMA Meteorological Observation Centre, Beijing* 100081, *China*

[5]*Beijing Municipal Meteorological Observation Center, Beijing* 102600, *China*

[6]*Qingdao Meteorological Comprehensive Support Center, Qingdao* 266003, *China*

(Received 25 September 2023; revised 14 March 2024; accepted 2 April 2024)

ABSTRACT

As a new type of wind field detection equipment, coherent Doppler wind lidar (CDWL) still needs more relevant observation experiments to compare and verify whether it can achieve the accuracy and precision of traditional observation equipment in urban areas. In this experiment, a self-developed CDWL provided four months of observations in the southern Beijing area. After the data acquisition time and height match, the wind profile data obtained based on a Doppler beam swinging (DBS) five-beam inversion algorithm were compared with radiosonde data released from the same location. The standard deviation (SD) of wind speed is 0.8 m s^{-1}, and the coefficient of determination R^2 is 0.95. The SD of the wind direction is 17.7° with an R^2 of 0.96. Below the height of the roughness sublayer (about 400 m), the error in wind speed and wind direction is significantly greater than the error above the height of the boundary layer (about 1500 m). For the case of wind speeds less than 4 m s^{-1}, the error of wind direction is more significant and is affected by the distribution of surrounding buildings. Averaging at different height levels using suitable time windows can effectively reduce the effects of turbulence and thus reduce the error caused by the different measurement methods of the two devices.

Key words: coherent Doppler wind lidar, radiosonde, wind measurement, urban boundary layer

Citation: Luo, Z. X., X. Q. Song, J. P. Yin, Z. C. Bu, Y. B. Chen, Y. T. Yu, and Z. L. Zhang, 2024: Comparison and verification of coherent Doppler wind lidar and radiosonde data in the Beijing urban area. *Adv. Atmos. Sci.*, https://doi.org/10.1007/s00376-024-3240-9.

Article Highlights:

- CDWL five-beam measurements were used to obtain wind field data in urban areas, which were compared with radiosonde data over an extended period.
- The correlation of wind speed and wind direction within the roughness sublayer is obviously poorer, owing to the effects of turbulence.
- The error in wind direction is highly influenced by the layout of the surrounding buildings, resulting in larger errors at lower wind speeds.
- The time average window for wind direction should be smaller than that for wind speed, and the time window needs to decrease with height.

1. Introduction

Atmospheric wind fields are among the more important meteorological elements directly affecting people, especially since they govern airflow through urban areas. They are further known to be the most important factor affecting human health, outdoor and indoor comfort, air quality, and the energy performance of buildings (Gao et al., 2012). By receiving the backscattered signal from atmospheric aerosols and mixing it with the local oscillation beam, Coherent Doppler Wind Lidar (CDWL) can obtain the full phase, frequency,

* Corresponding author: Xiaoquan SONG
Email: songxq@ouc.edu.cn

and amplitude information contained within the signal (Vaughan et al., 1996) and then use this to retrieve the atmospheric wind field. Currently, CDWL is one of the more important remote sensing devices for three-dimensional atmospheric wind field detection under non-precipitating conditions. It is widely used to measure atmospheric wind fields, atmospheric turbulence, convective observations, and predict extreme weather, such as storms. Compared with microwave weather radar, CDWL has a shorter wavelength, higher measurement accuracy, higher range resolution, and smaller beam divergence angle, which can better track the target. CDWL not only has the ability of wind cups and wind vanes to observe the wind field throughout the day but also has the ability of a radiosonde to measure the high-altitude atmosphere. As a kind of remote sensing instrument, CDWL also has the capability of sonic anemometers or acoustic radar to measure the three-dimensional atmospheric wind field.

In the global observing system, supplementary observations of high-altitude winds on land mainly use radiosondes, wind profilers, and Doppler weather radar (WMO, 2020). To fully understand the accuracy and precision of the data detected by a CDWL, a new wind field detection device, researchers have tested and analyzed its performance through a number of experiments. To reduce the impact of complex environmental conditions, most of the validation analyses of CDWL data are from flat and open areas. In addition to a comparison of lidar data with radiosonde (Hooper and Eloranta, 1986; Roadcap et al., 2001; Kumer et al., 2014; Ruchith et al., 2014; Mariani et al., 2020), the wind speed and wind direction data measured by wind cup, wind vane (Devara et al., 2015), sonic anemometers (Köpp et al., 1984), and wind profile radar (Ishii et al., 2005; Pearson et al., 2009; Päschke et al., 2014) were also used simultaneously for synergistic comparison and verification. The results show good consistency, indicating that lidar is capable of good wind measurement performance. Moreover, validation of airborne CDWL (Bucci et al., 2018) and shipborne CDWL (Wolfe et al., 2007; Achtert et al., 2015) was also conducted, and the results all show the performance and potential of CDWL as a wind field detection device. Except for the months or years-long comparison between CDWL and meteorological towers in the wind power industry, many observation experiments have a short period, making it difficult to encounter some special atmospheric environments during these experiments and verify the long-term CDWL detection accuracy. Some scholars have also studied the wind measurement capability of CDWL in urban areas (Lane et al., 2013; Dai et al., 2020), but comparison verification is mostly with wind cups, wind vane, and sonic anemometers; thus, the comparison height is limited by the height of meteorological towers and buildings.

This study is based on simultaneous wind field observation experiments from May to August 2020. The L-band sounding radar data from the Beijing Nanjiao Meteorological Observatory of the China Meteorological Administration (CMA) are used as the benchmark to compare and analyze CDWL data. Measurement accuracy and precision of wind field detection by a CDWL in the urban area of Beijing are analyzed. The remainder of this paper is organized as follows. Section 2 describes the experimental site, the CDWL and radiosonde equipment used, and outlines the research methodology. Section 3 describes the differences between the CDWL and radiosonde wind measurements for different wind speeds, directions, and heights, as well as the effect of time averaging on the CDWL data. Section 4 summarizes and concludes the results of the comparison between CDWL and radiosonde.

2. Methods

2.1. *Experiment overview*

This simultaneous observation experiment was carried out at the Beijing Nanjiao Meteorological Observatory of the CMA (Fig. 1) (39°48′22″N, 116°28′5″E, 32 m above sea level), where the CDWL was located 170 m away from the radiosonde release site. There are tall buildings (heights ≈ 40–80 m) within 1 km of the observation site in the northwest, west-southwest, south, and southeast directions. Trees and open space are mostly within 1 km in the southwest and east directions. The simultaneous observation experiment lasted for a total of 123 days (from 1 May 2020 to 31 August 2020). The CDWL was turned on 24 hours a day, covering a total of 246 radiosonde observations (released twice daily at 0715 and 1915 LST, LST=UTC+8).

2.2. *CDWL*

The system adopts the Wind3D 6000 CDWL jointly developed by the Ocean University of China and Qingdao Leice Transient Technology Co. LTD, and its performance specifications are given in Table 1. The Wind3D 6000 works in the infrared band, which is invisible to the human eye, and ideally enables three-dimensional atmospheric wind field and wind profile detection from the ground to a 6000 m radial distance. Since the experimental site is in an urban area, the atmospheric wind field close to the surface usually changes rapidly due to the influence of buildings and human activities. Therefore, the system uses Doppler beam swing (DBS) five-beam scanning measurement to obtain wind profiles. Compared to the velocity azimuth display (VAD) and range height indicator (RHI) methods, this instrument requires less scanning direction and obtains wind profile data with a higher temporal resolution.

The DBS is measured in five directions to retrieve the horizontal wind field, in which the radial wind speed is measured in the east, west, south, and north directions with a fixed elevation angle, and the fifth one to the zenith. The measurement accuracy of the scanning CDWL is not too sensitive to the elevation angle setting (Shimada et al., 2020). If the elevation angle is too small in urban areas, the scanning beam will be blocked by the surrounding buildings. Yet, an elevation angle that is too large will make the measurement data

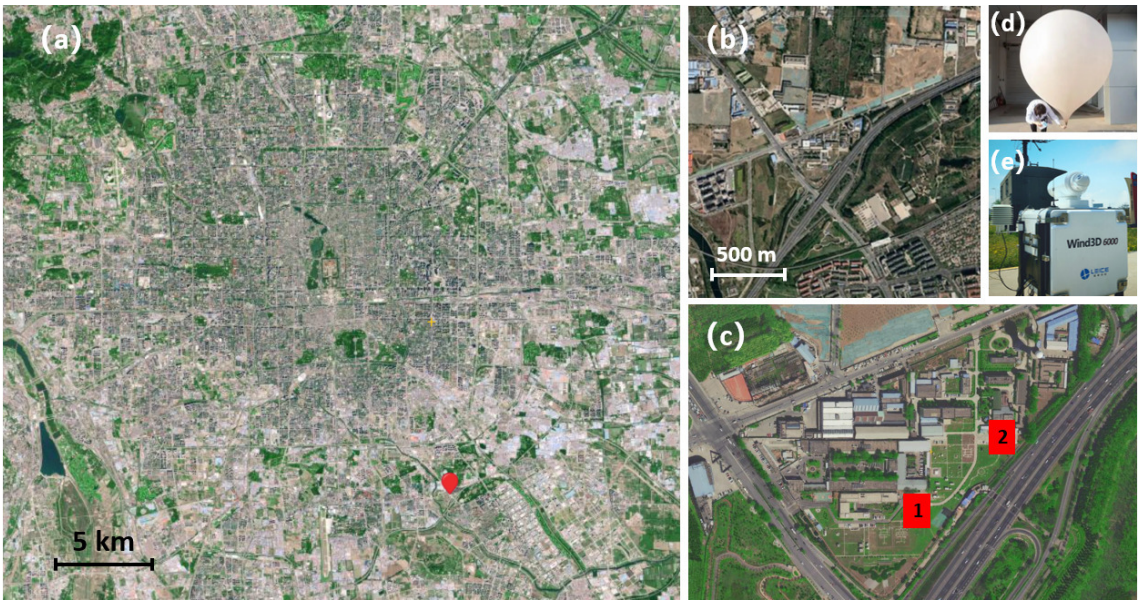

Fig. 1. Experimental sites and equipment situation. (a) Images of Beijing city, with the experimental site marked in red. (b) A partial image of the 2 km × 2 km area centered on the experimental site. (c) Enlarged view of the experimental site (label 1 is the location of the radiosonde balloon release, and label 2 is the location of the CDWL deployment). (d, e) Photos of the radiosonde balloon and CDWL equipment, respectively.

Table 1. CDWL and Radiosonde specifications.

Parameters	CDWL (Wind3D 6000)	Radiosonde (GTS11)
Measurement range	0–6000 m	0–40 000 m
Data sampling rate	~0.3 Hz	1 Hz
Range resolution	26 m	5–6 m

less representative. Lane et al. (2013) used an elevation angle of 75° in consideration of the fact that the experimental site was located in the center of London, where the height and density of buildings were larger; thus, a larger elevation angle was necessary to ensure that the beam was not blocked. In light of such considerations, this experiment uses a fixed elevation angle of 60° for DBS scanning. The wind profile obtained after scanning is retrieved from 51 m above the ground, with a vertical resolution of 26 m and a temporal resolution of 3–4 s.

2.3. *Radiosonde*

The radiosonde wind profile data was obtained from Beijing Nanjiao Meteorological Observatory, a station participating in the Global Conventional Weather Data Exchange (code 54511). Using the GTS11 digital radiosonde, it provides in-situ measurements of atmospheric environmental variables, including parameters such as temperature, pressure, relative humidity, wind speed, and wind direction (Xu et al., 2021) (see Table 1 for details). The L-band GFE(L)1 secondary radar is used for wind profile measurements. The radar calculates the movement speed and orientation of the radiosonde during the ascent by tracking and measuring the azimuth, pitch, and distance information, thus allowing it to measure wind speed and direction.

2.4. *Data matching*

In terms of measurement methods, a radiosonde and CDWL represent two different wind measurement techniques. CDWL measures the wind field in the scanning area at a fixed position (Eulerian measurement), while the radiosonde moves with the atmospheric wind field as the sounding balloon rises (Lagrangian measurement) (Roadcap et al., 2001). Thus, CDWL winds are captured from a limited range of resolutions, and CDWL winds at different altitudes represent different scales, whereas wind measurements by radiosondes are purely point measurements. The height, time, and scales of the wind profile detected by a CDWL and radiosonde may indeed be different (Kottayil et al., 2016). To make the data of the two instruments more reasonable for comparison, this experiment takes the time and height of the radiosonde data as a baseline and then finds the height layer and performs a time matching of the CDWL data. Taking the data matching of a radiosonde wind profile as an example, the first step is determining the height layer of the CDWL data closest to the radiosonde height. Here, the height difference is not more than 3 m (half of 5–6 m, the height of the radiosonde's rise per second) to avoid one CDWL data matching multiple radiosonde data. In the second step, for different time series

of CDWL wind profiles, the wind field data with the closest detection time in the above-matched height layer are identified for time matching, and the detection time difference between the two data does not exceed 3 s. It is worth noting that the height and time of the two measurement methods are closely matched. Still, most of them do not come from the same spatial position, which is a consequence of the relatively fixed vertical observation of the CDWL and the drift of the radiosonde in space with the wind. Figure 2 shows the box plot of the signal-to-noise ratio (SNR) of the CDWL measurements with height during the observation period. The SNR gradually decreases as the height increases, which is due to the inverse correlation between aerosol concentration and laser energy and height. When the SNR is less than 10 dB, the data is considered to be greatly affected by the noise in the signal. While using three-beam and two-beam methods (Song et al., 2021) or reducing the vertical resolution (Wang et al., 2021) can increase the amount of available data by improving the detection probability, it also yields an increase in bias. Therefore, in this paper, data with a SNR less than 10 dB are rejected for quality control.

In the wind direction comparison of the atmospheric wind field, if the statistical operator is calculated directly, the 0° and 360° boundary data will greatly impact the calculation results. The use of Eqs. (1) and (2) eliminates the effect of the 360° boundary, and the wind direction difference does not exceed 180°.

$$\delta = D_{\mathrm{L}} - D_{\mathrm{R}}\,, \tag{1}$$

$$\Delta = \begin{cases} \delta - 360, & \delta > 180^\circ \\ \delta, & -180^\circ \leqslant \delta \leqslant 180^\circ \\ \delta + 360, & \delta < -180^\circ \end{cases}, \tag{2}$$

where D_{L} is the wind direction measured by the CDWL, D_{R} is the wind direction measured by the radiosonde, δ is the absolute wind direction difference between the two, and Δ is the wind direction difference after eliminating the boundary effect.

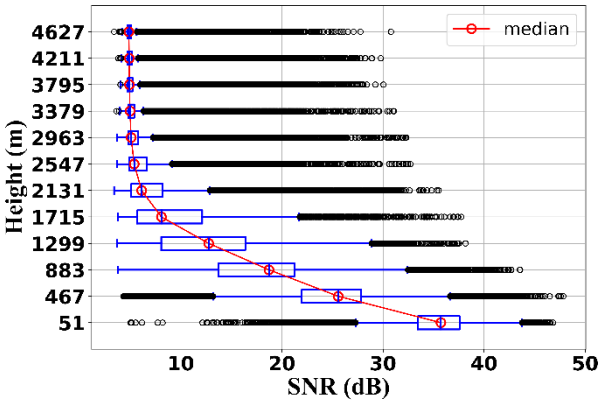

Fig. 2. Boxplot of CDWL SNR (the red circle is the median). When the SNR is less than 10 dB, the line-of-sight measurement is rejected by data quality control.

A total of 234 sets of simultaneous wind profiles (instead of 246 sets) were obtained by the CDWL. This was because 10 sets of the simultaneous wind profiles had lidar failures. Two other sets (1915 LST on 11 May 2020 and 1915 LST on 24 June 2020) were affected by a rapid decrease in visibility and rainfall, respectively, resulting in a serious distortion of wind speed; thus, these data were rejected. A decrease in visibility may be caused by the rapid increase in aerosol concentration in the atmosphere, and rapid changes in aerosol concentration have been shown to significantly impact the measurement error of a CDWL (Dai et al., 2020). The latter may be due to rainfall that causes the bimodal peaks to be detected in the Doppler spectrum of the CDWL (Träumner et al., 2009), leading to a misjudgment of the wind speed. In summary, the subsequent analysis discussion in this paper is based on 234 sets of matched data after the removal of missing and erroneous data.

2.5. *Quality metrics used for evaluation and wind averaging calculations*

The following describes the evaluation metrics used in this paper to evaluate the wind measurement capability of CDWL:

$$\mathrm{BIAS} = \frac{\sum_{i=1}^{n}(V_{\mathrm{L}i} - V_{\mathrm{R}i})}{n}\,, \tag{3}$$

$$\mathrm{MAE} = \frac{\left|\sum_{i=1}^{n}(V_{\mathrm{L}i} - V_{\mathrm{R}i})\right|}{n}\,, \tag{4}$$

$$\mathrm{SD} = \sqrt{\frac{\left(\sum_{i=1}^{n}(V_{\mathrm{L}i} - V_{\mathrm{R}i})\right)^2}{n}}\,. \tag{5}$$

Equations (3)–(5) represent the bias, mean absolute deviation (MAE), and SD of the wind speed, respectively, where $V_{\mathrm{L}i}$ and $V_{\mathrm{R}i}$ are the matched wind speeds from the CDWL and radiosonde, respectively. Note that $V_{\mathrm{L}i} - V_{\mathrm{R}i}$ is replaced with Δ, described in Eqs. (1–2), when calculating the wind direction.

Equations (6)–(10) are used for wind-sliding averages:

$$u = -\frac{1}{N}\sum_{i=1}^{N} V_i \sin(D_i)\,, \tag{6}$$

$$v = -\frac{1}{N}\sum_{i=1}^{N} V_i \cos(D_i)\,, \tag{7}$$

$$V = \sqrt{u^2 + v^2}\,, \tag{8}$$

$$D = \mathrm{mod}\left(180 + \frac{180}{\pi}\arctan2(u, v), 360\right), \quad (9)$$

where mod stands for the modulo function to get an answer in degrees in the range $0 \leqslant D < 360$, V_i and D_i are the wind speed and direction of the CDWL, respectively, and u and v are the zonal and meridional components of the averaged wind, respectively. The averaged wind speed and direction are then calculated according to Eqs. (8) and (9).

3. Results and discussion

3.1. *CDWL observation results*

The comparison of wind speed and wind direction (Fig. 3) between CDWL and radiosonde observations was performed from May to August 2020 after the data matching described in the last section. In 234 sets of wind profile matching, a total of 11390 data pairs were obtained. The statistical bias of wind speed was 0.2 m s^{-1}, the standard deviation (SD) was 0.8 m s^{-1}, the mean absolute deviation (MAE) was 0.6 m s^{-1}, and the coefficient of determination R^2 was 0.95. In Fig. 3b, the polar coordinate angle is the wind direction measured by the CDWL, and the radius is denoted Δ. The bias of the wind direction is less than 1°, the SD is 17.7°, the MAE is 9°, and the coefficient of determination R^2 is 0.96. Wind speed comparison results are similar to Köpp et al. (1984), Päschke et al. (2014), and Roadcap et al. (2001). However, in the wind direction comparison, the SD is 5°–7° larger than their results. This may be due to the locations of their test sites being in relatively flat and open areas, so the atmospheric wind field is more consistent in terms of wind direction at all heights.

3.2. *Effect of SNR*

The signal-to-noise ratio (SNR) is an important parameter of CDWL detection as it directly affects the accuracy of wind velocity retrieval. In general, too low of an SNR will cause the effective signal to be covered by noise, making it difficult to estimate the true Doppler shift, thus increasing the error of the retrieved radial wind speed (Smalikho, 2003). To investigate the effect of the SNR on measurement accuracy, the SNR was divided every 3 dB as a numerical interval, from which the bias of wind speed and direction in each interval was calculated (Figs. 4a, b). The blue dots in Fig. 4 are the bias for each pair of matching data, the red hollow circles are the median of the bias in each value interval, and the red triangles are the mean of the bias. The upper bound of the boxplot is the upper quartile of the SNR in each interval plus 1.5 times the interquartile range, and the lower bound is the lower quartile minus 1.5 times the interquartile range. It can be seen that when the SNR is greater than 10 dB, its variation has little effect on the measurement accuracy of wind speed and wind direction. In each interval, the average bias of wind speed is close to 0 m s^{-1}, and the average bias of wind direction is also around 0°. This result also proves that the data retained after the removal of data with an SNR less than 10 dB during data preprocessing can estimate the true Doppler shift, and then retrieve the radial wind speed. With increased SNR, although the mean value does not change much, the wind bias becomes more discrete. This may be partially due to the general trend of the SNR of the CDWL being inversely proportional to height, and the high roughness nature in urban areas makes it easy to cause high-intensity turbulence in the wind field close to surface height. So, even if the SNR is relatively high, it affects the magnitude of wind direction bias. The increase in bias in the last three SNR intervals for wind speed and direction may be caused by the small number of data pairs (33, 5, and 1 in the last three bins, respectively).

3.3. *Differences in different detection heights*

Unlike flat terrain, urban areas have more numerous and taller building blocks. Wind fields can be directly affected by rough surfaces (e.g., buildings, trees) to form turbulence and exhibit large variations in the horizontal and verti-

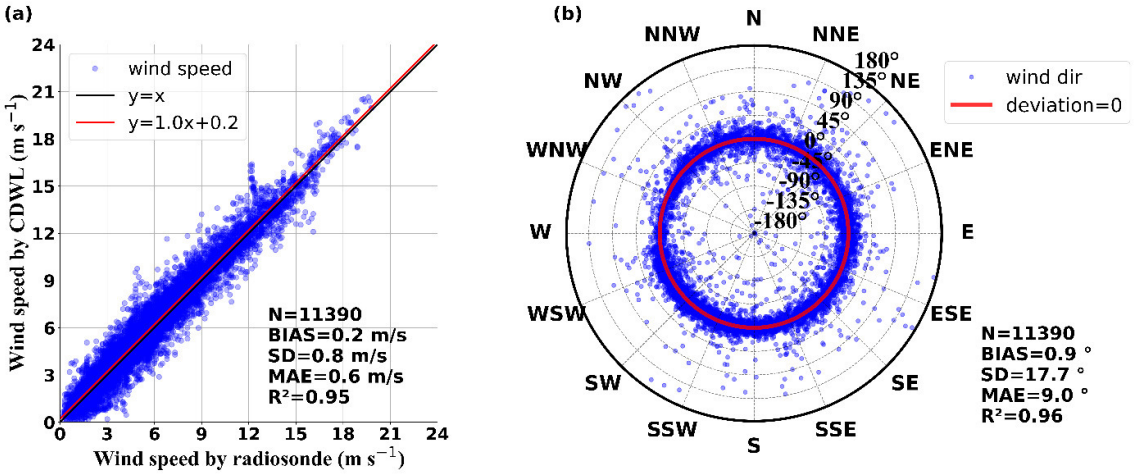

Fig. 3. Scatterplots of (a) full height wind speed and (b) wind direction from May to August 2020.

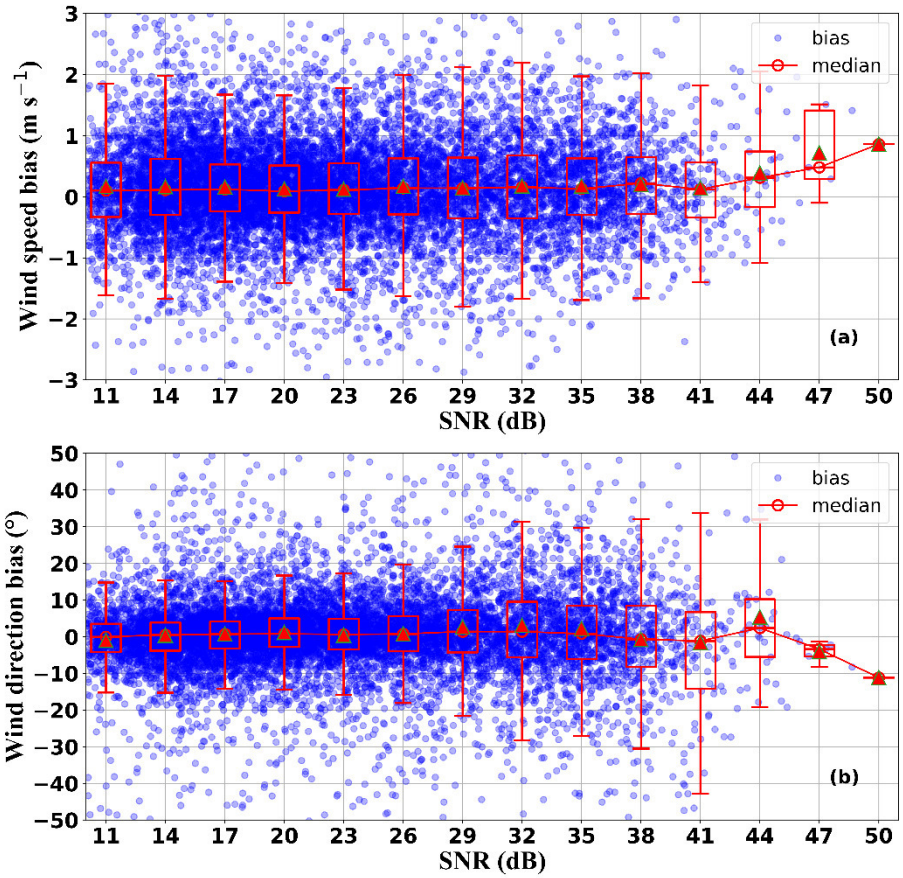

Fig. 4. Box plots of (a) wind speed and (b) wind direction biases as a function of SNR. The statistics for each box plot are calculated within a 3 dB SNR bin.

cal ranges. This can cause discrepancies in wind field measurements by CDWL and radiosondes. The height of the roughness sublayer is generally 2–5 times the height of buildings or trees (Raupach et al., 1991), and the wind field within this height is most affected by buildings. In this paper, the roughness sublayer height is set equal to five times the height of the tallest building (~80 m) within 1 km around the experimental site. Wind fields above the height of the roughness sublayer are also affected by surface friction until the height rises to the planetary boundary layer height (PBLH). The wind field above the PBLH can then be considered as the free atmosphere, a layer no longer affected by friction.

Based on four months of radiosonde data, the PBLH in Beijing was calculated and recorded using the potential temperature gradient method, as shown in Fig. 5 (Seidel et al., 2010). The width of the shapes indicates the density of data point distribution, a greater width represents a higher density of data points. The white dots in the center are the medians of the statistics, which are 1494 m, 1071 m, and 1912 m, respectively, and the mean values of the PBLH are 1693 m, 1456 m, and 1930 m for the three cases, respectively. The median value of the overall PBLH (~1500 m) is used as the height division, considering the effects of the boundary layer and radiosonde drift on the CDWL wind measurement comparison. In this paper, the CDWL-matched data are divided into three height regions (0–400 m, 400–1500 m, >1500 m), respectively; thus, allowing for the wind speed and wind direction deviations representative of the roughness sublayer, PBL, and free atmosphere to be studied.

As can be seen from Fig. 6, the wind speed measured by the CDWL was slightly greater than that measured by the radiosonde at all heights. This may be because the wind speed is positively correlated with the height above ground, while the inertial effect of radiosonde itself requires an acceleration process within the atmospheric wind field (Zhou et al., 2022). This may reduce its ability to truly reflect the instantaneous wind speed of the scene, thus causing deviations between the two devices. As the detection altitude moves from the roughness sublayer near the ground to the free atmosphere at high altitudes, the wind speed correlation between the two devices first increases and then decreases slightly. This is due to turbulence being easily generated within the roughness sublayer, owing to terrain friction and the effects of surface buildings. When the radiosonde passes through small-scale turbulence during its ascent or the CDWL scans this small-scale turbulence, it will cause an error in both measurements. Although the height above the roughness sublayer and below the PBL is also affected by surface friction, it is much less affected than that of the roughness

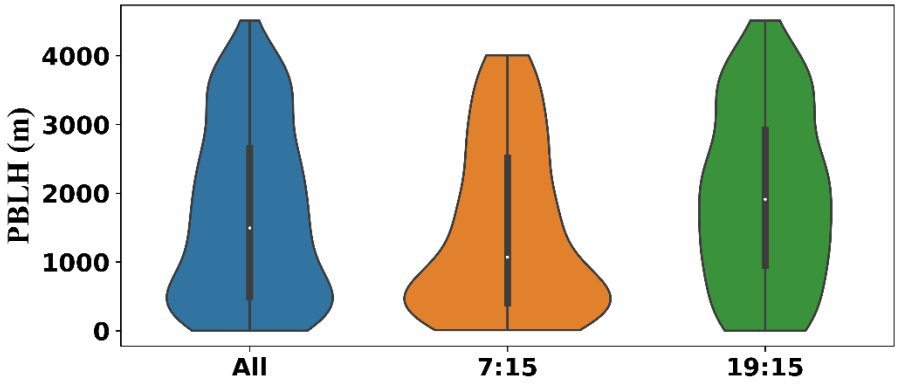

Fig. 5. Planetary boundary layer height (PBLH) at different times. 7:15 and 19:15 on the *x*-axis represent radiosondes launched around 0715 and 1915 LST, respectively. ALL represents radiosondes that include both 0715 and 1915 LST.

sublayer. When the detection height is higher than ~1500 m of the PBLH, the radiosonde gradually moves away from the detection range of the CDWL as the height increases. The slight decrease in wind speed correlation may result from the horizontal homogeneity of the atmosphere being relatively poor for the summer experiment period (Tian and Lü, 2017). The SD of wind direction for both devices in Fig. 7 decreases significantly with altitude, and the wind direction error in the free atmosphere is much less affected by sounding drift than wind speed. This result also shows that CDWL data fits well with the wind field measured by a radiosonde in a constant flow environment.

3.4. *Influence of different wind speeds and directions*

To investigate the measurement capability of CDWL at different wind speeds, Fig. 8 shows the SD of wind speed and wind direction in each interval calculated by taking every 1 m s^{-1} of wind speed measured by the radiosonde as an interval. The number above each interval is the number of samples in the interval. When the number of samples is less than 10, the amount of data is considered insufficient to reflect the wind field; therefore, no calculation is performed. From the results of the three height ranges of 0–400 m, 400–1500 m, and >1500 m, it can be seen that at altitudes within 1500 m, the SD of wind speed slowly increases with the increase of wind speed. There is no significant pattern for the SD change of wind speed above 1500 m. The SD of wind direction in all height ranges decreases rapidly in the interval of 0–4 m s^{-1} and then remains stable. The main reason for this phenomenon may be that the radiosonde does not change its motion as quickly as it does at high wind speeds, and it takes some time to match the ambient wind field when the wind direction changes.

Since the experimental site is in an urban area, the measurement data of the radiosonde and CDWL are easily affected by the distribution of surrounding buildings. Figure 9 shows the SD of wind speed and wind direction for each 22.5° interval as calculated by the wind direction measured by a radiosonde. Figure 9a clearly shows that the SD of wind direction varies significantly in different directions. In the interval of 250°–360°, the SD of wind direction even exceeds 30°, and the SD of wind speed is also higher than the average value between 300° and 360°. This directional range is precisely in the direction of dense building clusters within 1 km from the experimental site, and it is also in the direction of the main urban area of Beijing. Among them, the buildings in the west-southwest (247.5°–270°) direction are the tallest buildings (about 80 m) within a 1 km distance from the experimental site, corresponding to the peak SD of wind direction in Fig. 9a. There is a clear valley in the southwest direction at an altitude of 400–1500 m, which may explain why the local prevailing wind is southwesterly during the experiment. Notably, the radiosonde casting site is also southwest of the CDWL deployment site; thus, a southwesterly wind will blow the radiosonde over the CDWL, potentially causing the measured values of the two devices to be closer. At the same time, there are mostly trees and open space within 1 km southwest of the experimental site, which has less influence on the wind field.

3.5. *Effect of the average time of CDWL data*

Atmospheric inhomogeneity caused by turbulence is an important factor contributing to CDWL measurement errors (Gasch et al., 2020). Urban areas are characterized by high roughness and large sensible heat flux, with higher turbulent kinetic energy (Qian et al., 2022). Averaging over a certain period of time effectively reduces the inconsistency of measurements caused by turbulence between the two devices (Tang et al., 2022). Figure 10 shows the difference in the SD of wind speed and direction for each height range after a sliding average of the matched data compared to the SD before the sliding average. Sliding time windows of 1, 2, 3, 6, 10, and 20 minutes were applied. The wind field averaging method adopts vector averaging, decomposes the original wind field data into *u*- and *v*- components for a sliding average, and then synthesizes the components into the new wind field data. From Fig. 10a, it can be seen that the wind speed SD becomes smaller compared to the original wind speed SD at all height levels within time windows having less than a 10-min average, especially for height ranges of

0–400 m and above 1500 m. However, when a 20-min sliding average is performed, the SD of wind speed in the 400–1500 m range no longer decreases with an increase of the average time window. This implies that the averaging

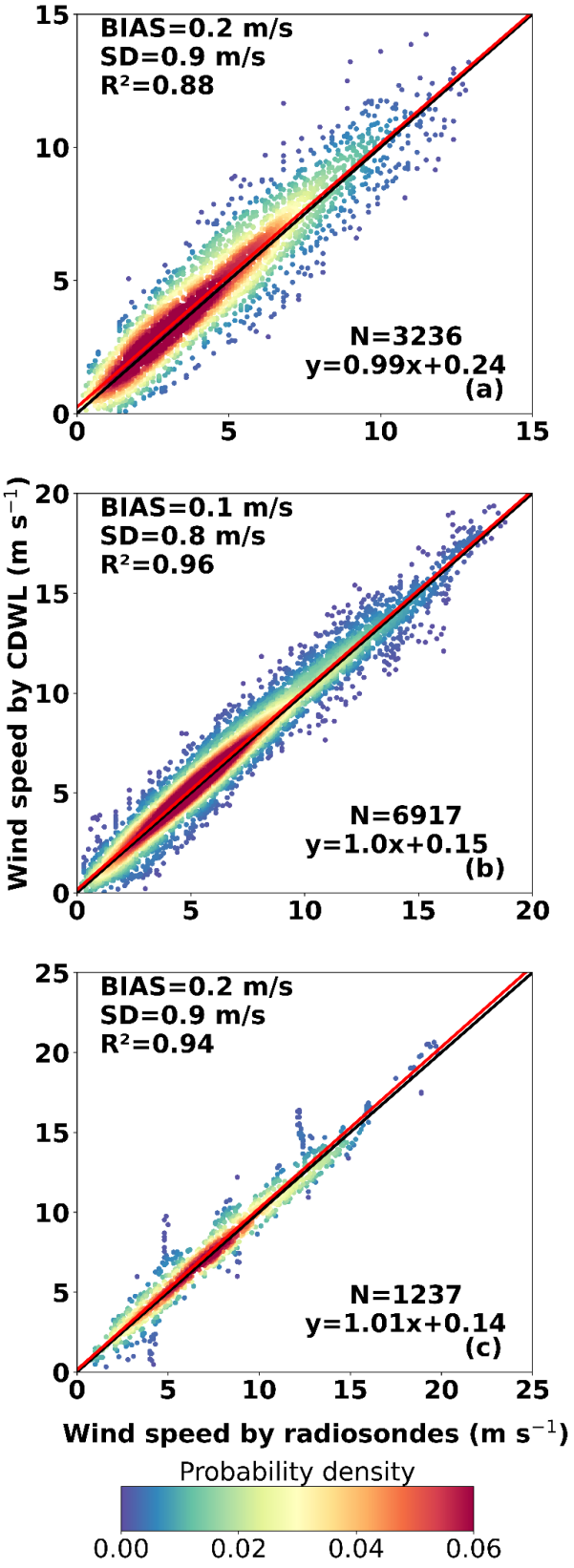

Fig. 6. Scattered density plot for wind speed comparison for heights (a) 0–400 m, (b) 400–1500 m, and (c) above 1500 m.

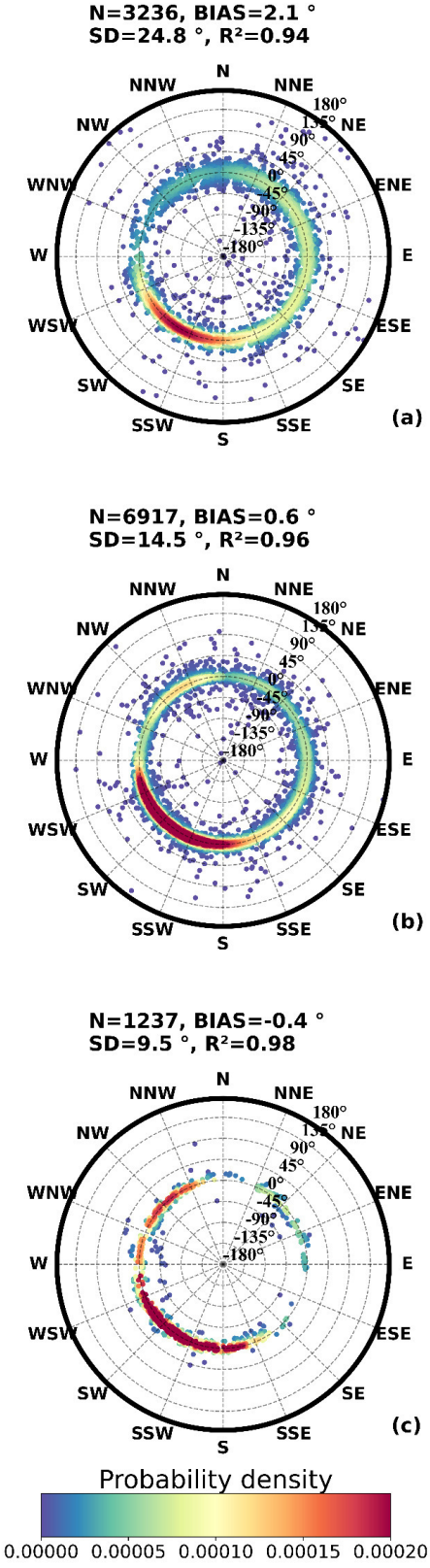

Fig. 7. Scattered density plot for wind direction comparison for heights of (a) 0–400 m, (b) 400–1500 m, and (c) above 1500 m, respectively.

time window should not be expanded but rather be adapted to the local environmental and meteorological conditions. From the wind direction time averaging results (Fig. 10b), it can be seen that using 6- and 10-min time windows is optimal below 1500 m. The averaging of 2- and 3-min time windows yields a very good optimization effect on the wind direction for the heights above 1500 m. In summary, when using time averaging to eliminate turbulence effects, longer time averaging (10 to 20 min) can be used for wind speed; however, longer time averaging is not recommended for wind direction, and the averaging time window can be reduced appropriately at heights from the near-surface layer to the high-altitude

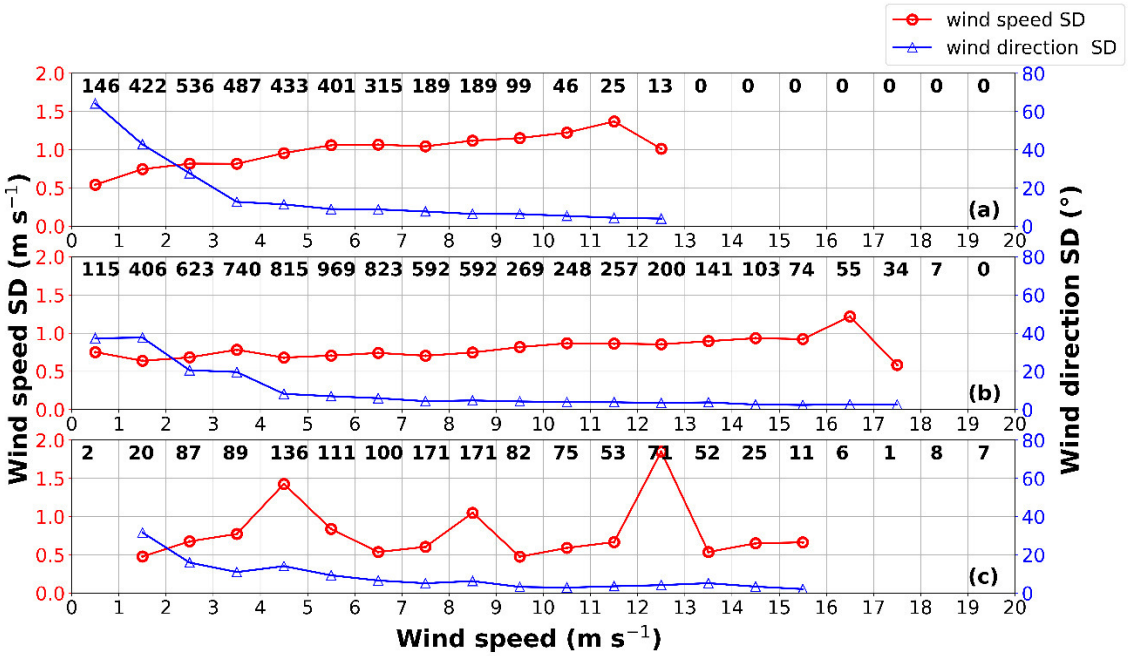

Fig. 8. The SD of wind speed and wind direction calculated according to a 1 m s^{-1} interval of wind speed as measured by a radiosonde. The red circle is the SD of wind speed, and the hollow blue triangle is the SD of wind direction. Panels (a, b, c) show the three height intervals (0–400 m, 400–1500 m, >1500 m), respectively.

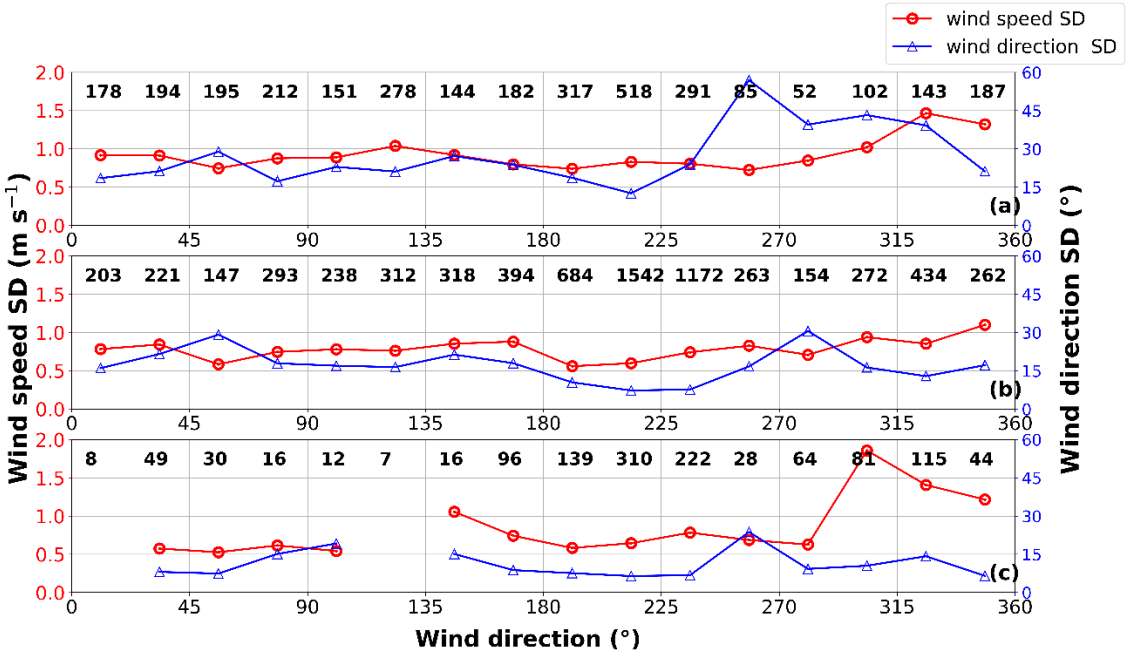

Fig. 9. SD of wind speed and wind direction calculated according to a 22.5° wind direction interval as measured by a radiosonde. The red circle is the SD of wind speed, and the blue hollow triangle is the SD of wind direction. Panels (a, b, c) show the three height intervals (0–400 m, 400–1500 m, >1500 m), respectively. The number above each bin is the number of samples in the interval.

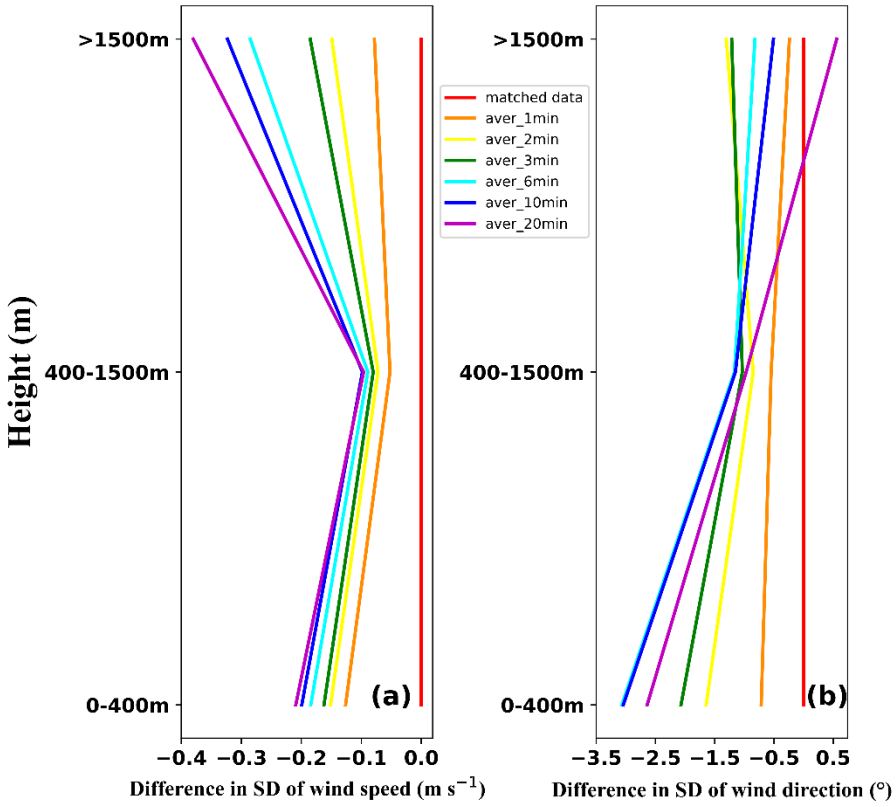

Fig. 10. Comparison of SD differences in (a) wind speed and (b) direction between different time windows of the sliding average method. The difference in SD is defined as the SD after the sliding average—the SD before the sliding average, demonstrating how much the sliding average reduces SD.

layer.

4. Summary and conclusions

The Wind3D 6000 CDWL was operated with continuous DBS scanning at a 60° elevation angle in Beijing from May to August 2020. The obtained atmospheric wind profile data were compared with radiosonde measurements deployed twice daily. A total of 234 sets of usable matching data were obtained, with detection heights up to 5000 m. The failure rate of the CDWL during the unattended experiment was 4.8%. Compared with a radiosonde, the SD of wind speed was 0.8 m s^{-1}, and the SD of wind direction was 17.7°, respectively. The mean bias of wind speed was 0.2 m s^{-1}, and the mean bias of wind direction was 0.9°, respectively.

The bias of CDWL data in different SNR intervals was calculated separately. The results proved that data with an SNR greater than 10 dB during quality control can correctly reflect the atmospheric wind field in the Beijing urban area. The comparison with the radiosonde reveals that the wind speed and direction clearly tend to decrease SD with increased altitude. This is due to the turbulence generated by surface friction, an effect amplified in urban areas by surface objects, particularly for wind direction measurements. At heights above the PBL, the wind speed error will increase slightly due to the drift of the radiosonde. However, on the whole, the data measured by the two devices are in agreement.

The measurement errors of wind speed and wind direction are also affected by the distribution of buildings. When tall buildings are in the upwind direction, errors are easily generated, especially within the height of the roughness sublayer. When the wind speed is less than 4 m s^{-1}, it is easy for the wind direction error to increase. This is due to the inertia of the radiosonde, which cannot correctly reflect the instantaneous wind field at small wind speeds.

Time averaging of CDWL data can eliminate the effect of atmospheric inhomogeneity caused by turbulence, thus achieving better consistency in the wind speed and direction measured by the two devices. This experiment shows that upon selecting the time-averaging window for Beijing, it is recommended to choose a window of 10 to 20 min for wind speed averaging, while the time averaging window for wind direction can be less than 10 min. The time averaging window with altitude rise can be appropriately reduced to 2 to 3 min.

Experiments show that 5-beam DBS scanning of CDWL is suitable for long-term deployment measurements in urban areas. This method can solve the problems of sparse radiosonde observation data and low detection height of fixed wind cups, wind vanes, and sonic anemometers. Advantages of CDWL include, but are not limited to, its

small dimensions, low power consumption, use of invisible wavelengths that are safe for human eyes, and zero negative impacts from electromagnetic radiation or noise. This makes it suitable for station observation in urban areas and for providing atmospheric wind field data with a high spatial and temporal resolution for urban regional meteorological services, wind engineering, and urban environmental applications.

Acknowledgements. We sincerely thank the Meteorological Observation Centre of the China Meteorological Administration for organizing this observation campaign and the Meteorological Observation Centre of Beijing for providing the radiosonde data. This work was financially supported by the National Key R&D Program of China (2022YFC3700400 & 2022YFB3901700).

REFERENCES

Achtert, P., I. M. Brooks, B. J. Brooks, B. I. Moat, J. Prytherch, P. O. G. Persson, and M. Tjernström, 2015: Measurement of wind profiles by motion-stabilised ship-borne Doppler lidar. *Atmospheric Measurement Techniques*, **8**(11), 4993–5007, doi: 10.5194/amt-8-4993-2015.

Bucci, L. R., C. O'Handley, G. D. Emmitt, J. A. Zhang, K. Ryan, and R. Atlas, 2018: Validation of an airborne Doppler wind lidar in tropical cyclones. *Sensors*, **18**(12), 4288, https://doi.org/10.3390/s18124288.

Dai, L. D., and Coauthors, 2020: Multilevel validation of Doppler wind lidar by the 325 m meteorological tower in the planetary boundary layer of Beijing. *Atmosphere*, **11**(10), 1051, https://doi.org/10.3390/atmos11101051.

Devara, P. C. S., Y. Jaya Rao, S. M. Sonbawne, M. G. Manoj, K. K. Dani, and S. K. Saha, 2015: First results of compact coherent Doppler wind lidar and its validation at IITM, Pune, India. *Meteorological Applications*, **22**(2), 156–164, https://doi.org/10.1002/met.1428.

Gao, Y. F., R. M. Yao, B. Z. Li, E. Turkbeyler, Q. Luo, and A. Short, 2012: Field studies on the effect of built forms on urban wind environments. *Renewable Energy*, **46**, 148–154, https://doi.org/10.1016/j.renene.2012.03.005.

Gasch, P., A. Wieser, J. K. Lundquist, and N. Kalthoff, 2020: An LES-based airborne Doppler lidar simulator and its application to wind profiling in inhomogeneous flow conditions. *Atmospheric Measurement Techniques*, **13**(3), 1609–1631, https://doi.org/10.5194/amt-13-1609-2020.

Hooper, W. P., and E. W. Eloranta, 1986: Lidar measurements of wind in the planetary boundary layer: The method, accuracy and results from joint measurements with Radiosonde and Kytoon. *J. Climate Appl. Meteorol.*, **25**(7), 990–1001, https://doi.org/10.1175/1520-0450(1986)025<0990:LMOWIT>2.0.CO;2.

Ishii, S., K. Mizutani, T. Aoki, M. Sasano, Y. Murayama, T. Itabe, and K. Asai, 2005: Wind profiling with an eye-safe coherent Doppler lidar system: Comparison with radiosondes and VHF radar. *J. Meteor. Soc. Japan*, **83**(6), 1041–1056, https://doi.org/10.2151/jmsj.83.1041.

Köpp, F., R. L. Schwiesow, and C. Werner, 1984: Remote measurements of boundary-layer wind profiles using a CW Doppler lidar. *J. Climate Appl. Meteorol.*, **23**(1), 148–154, https://doi.org/10.1175/1520-0450(1984)023<0148:RMOBLW>2.0.CO;2.

Kottayil, A., and Coauthors, 2016: Validation of 205 MHz wind profiler radar located at Cochin, India, using radiosonde wind measurements. *Radio Sci.*, **51**(3), 106–117, https://doi.org/10.1002/2015RS005836.

Kumer, V.-M., J. Reuder, and B. R. Furevik, 2014: A comparison of LiDAR and radiosonde wind measurements. *Energy Procedia*, **53**, 214–220, https://doi.org/10.1016/j.egypro.2014.07.230.

Lane, S. E., J. F. Barlow, and C. R. Wood, 2013: An assessment of a three-beam Doppler lidar wind profiling method for use in urban areas. *Journal of Wind Engineering and Industrial Aerodynamics*, **119**, 53–59, https://doi.org/10.1016/j.jweia.2013.05.010.

Mariani, Z., R. Crawford, B. Casati, and F. Lemay, 2020: A multi-year evaluation of Doppler lidar wind-profile observations in the arctic. *Remote Sensing*, **12**(2), 323, https://doi.org/10.3390/rs12020323.

Päschke, E., R. Leinweber, and V. Lehmann, 2014: A one year comparison of 482 MHz radar wind profiler, RS92-SGP Radiosonde and 1.5 µm Doppler Lidar wind measurements. *Atmospheric Measurement Techniques Discussions*, **7**, 11 439–11 479, https://doi.org/10.5194/amtd-7-11439-2014.

Pearson, G., F. Davies, and C. Collier, 2009: An analysis of the performance of the UFAM pulsed Doppler lidar for observing the boundary layer. *J. Atmos. Oceanic Technol.*, **26**(2), 240–250, https://doi.org/10.1175/2008JTECHA1128.1.

Qian, Y., and Coauthors, 2022: Urbanization impact on regional climate and extreme weather: Current understanding, uncertainties, and future research directions. *Adv. Atmos. Sci.*, **39**(6), 819–860, https://doi.org/10.1007/s00376-021-1371-9.

Raupach, M. R., R. A. Antonia, and S. Rajagopalan, 1991: Rough-wall turbulent boundary layers. *Applied Mechanics Reviews*, **44**(1), 1–25, https://doi.org/10.1115/1.3119492.

Roadcap, J. R., P. J. McNicholl, E. H. Teets, and M. H. Laird, 2001: Comparison of CO_2 Doppler lidar and GPS rawinsonde wind velocity measurements. *Proc. SPIE 4376, Laser Weapons Technology II*, Orlando, FL, USA, SPIE, 141–152, https://doi.org/10.1117/12.438174.

Ruchith, R. D., M. C. R. Kalapureddy, S. Deshpande, K. K. Dani, and P. Ernest Raj, 2014: Inter-comparison of wind profiles in the tropical boundary layer remotely sensed from GPS radiosonde and Doppler wind lidar. *Int. J. Remote Sens.*, **35**(9), 3300–3315, https://doi.org/10.1080/01431161.2014.902552.

Seidel, D. J., C. O. Ao, and K. Li, 2010: Estimating climatological planetary boundary layer heights from radiosonde observations: Comparison of methods and uncertainty analysis. *J. Geophys. Res.*, **115**(D16), D16113, https://doi.org/10.1029/2009JD013680.

Shimada, S., J. P. Goit, T. Ohsawa, T. Kogaki, and S. Nakamura, 2020: Coastal wind measurements using a single scanning LiDAR. *Remote Sensing*, **12**(8), 1347, https://doi.org/10.3390/rs12081347.

Smalikho, I., 2003: Techniques of wind vector estimation from data measured with a scanning coherent Doppler lidar. *J. Atmos. Oceanic Technol.*, **20**(2), 276–291, https://doi.org/10.1175/1520-0426(2003)020<0276:TOWVEF>2.0.CO;2.

Song, X. Q., W. R. Long, L. Yun, C. Lu, and J. P. Yin, 2021: Analysis of accuracy and acquisition rate of Doppler Lidar multi-beam wind measurement. *Acta Optica Sinica*, **41**(10), 9–16, https://doi.org/10.3788/AOS202141.1001001.

Tang, S. M., Y. Guo, X. Wang, J. Tang, T. T. Li, B. K. Zhao, S. Zhang, and Y. P. Li, 2022: Validation of Doppler wind lidar during super Typhoon Lekima (2019). *Frontiers of Earth Science*, **16**(1), 75−89, https://doi.org/10.1007/s11707-020-0838-9.

Tian, Y. F., and D. R. Lü, 2017: Comparison of Beijing MST radar and radiosonde horizontal wind measurements. *Adv. Atmos. Sci.*, **34**(1), 39−53, https://doi.org/10.1007/s00376-016-6129-4.

Träumner, K., J. Handwerker, A. Wieser, J. Grenzhäuser, and C. Kottmeier, 2009: Advantages of a coordinated scanning Doppler lidar and cloud radar system for wind measurements. *Proc. 4th Symp. on Lidar Atmospheric Applications*, Phoenix, AZ, USA.

Vaughan, J. M., K. O. Steinvall, C. Werner, and P. H. Flamant, 1996: Coherent laser radar in Europe. *Proceedings of the IEEE*, **84**(2), 205−226, https://doi.org/10.1109/5.482229.

Wang, L., W. Qiang, H. Y. Xia, T. W. Wei, J. L. Yuan, and P. Jiang, 2021: Robust solution for boundary layer height detections with coherent Doppler wind lidar. *Adv. Atmos. Sci.*, **38**(11), 1920−1928, https://doi.org/10.1007/s00376-021-1068-0.

WMO, 2020: Guide to instruments and methods of observation. WMO-No. 8.

Wolfe, D. E., and Coauthors, 2007: Shipboard multisensor merged wind profiles from the New England Air Quality Study 2004. *J. Geophys. Res.*, **112**(D10), D10S15, https://doi.org/10.1029/2006JD007344.

Xu, H., and Coauthors, 2021: The significant role of radiosonde-measured cloud-base height in the estimation of cloud radiative forcing. *Adv. Atmos. Sci.*, **38**(9), 1552−1565, https://doi.org/10.1007/s00376-021-0431-5.

Zhou, J., H. Gao, X. S. Wang, and J. B. Li, 2022: An accurate wind retrieval method based on observing hydrogen balloons with multi-theodolite measurements. *J. Atmos. Oceanic Technol.*, **39**, 1297−1307, https://doi.org/10.1175/JTECH-D-21-0150.1.